Applied Mathematics and Computation 314 (2017) 334–348

Contents lists available at ScienceDirect

Applied Mathematics and Computation

journal homepage: www.elsevier.com/locate/amc

A Decoupled method for image inpainting with patch-based low rank regulariztion☆

Fang Li[a], Xiaoguang Lv[b,*]

[a] Department of Mathematics, East China Normal University, Shanghai, China
[b] School of Science, Huaihai Institute of Technology, Lianyungang, Jiangsu, China

ARTICLE INFO

Keywords:
Image inpainting
Transform domain
Low rank
Weighted nuclear norm

ABSTRACT

In this paper, we propose a decoupled variational method for image inpainting in both image domain and transform domain including wavelet domain and Fourier domain. The original image inpainting problem is decoupled as two minimization problems with different energy functionals. One is image denoising with low rank regularization method, i.e., the patch-based weighted nuclear norm minimization (PWNNM). The other is linear combination in image domain or transform domain. An iterative algorithm is then obtained by minimizing the two problems alternatingly. In particular, we derive the variational formulas for PWNNM and reformulate the denoising process into three steps: image decomposition, patch matrix denoising, and image reconstruction. The convergence of the numerical algorithm is proved under some assumptions. The numerical experiments and comparisons on various images demonstrate the effectiveness of the proposed methods.

1. Introduction

Image inpainting is an important topic in computer vision and image processing. The problem occurs when the observed data is incomplete in the sense that some pixels or coefficients of the target image under certain transform are missing or corrupted [1,37]. The aim of image inpainting is to recover an ideal image from the incomplete data. Here the ideal image is expected to have edges, structures and texture patterns consistent with the given data in a natural way for human eyes [4].

Image inpainting can be classified into two classes: image domain inpainting and transform domain inpainting. The former means that some pixels in the image domain are missing, while the latter means that some coefficients in certain transform domain are missing. Image domain inpainting has widely applications in restoring ancient drawings and old pictures, where some pixels are missing or damaged due to aging or scratch, or in removal of objects in photography or films for special effects [1,11]. In many practical applications, since images are formatted, transmitted, stored or encoded as transformed coefficients of images in some transformed domain, the coefficients may be lost or corrupted and thus it leads to the transform domain inpainting problem. The widely used image transforms include discrete cosine transform (DCT) (e.g. Joint Photographic Experts Group (JPEG) image), wavelet transform (e.g. JPEG 2000 image), and Fourier transform (e.g. magnetic resonance (MR) imaging) [8,10], etc.

☆ This work is supported by by the National Natural Science Foundation of China (NSFC) (11671002, 61401172), the Science and Technology Commission of Shanghai Municipality (STCSM) (13dz2260400), and Qing Lan Project, NSF of HHIT (Z2015004).

* Corresponding author.
E-mail addresses: fli@math.ecnu.edu.cn (F. Li), xiaoguanglv@hhit.edu.cn (X. Lv).

http://dx.doi.org/10.1016/j.amc.2017.06.027
0096-3003/

In recent years, many useful techniques have been developed to solve the image domain inpainting problem. These methods can be roughly classified into pixel based methods and exemplar based methods. In the pixel based methods, the missing region is filled by diffusing the image information from the known region to the missing region pixel by pixel via some partial differential equations (PDEs) [1,2,13,28,29], or by updating the sparse representation coefficients of the image under certain transforms such as wavelet, tight frame or dictionary [4,14,16,19,23,27,38]. In the exemplar based inpainting methods, the missing region is filled by propagating the image information in the known region patch by patch [11,35,36].

The transform domain inpainting problem has also been widely studied using variational methods, especially wavelet domain inpainting and Fourier domain inpainting. In the variational methods, the regularization scheme plays a leading role. Chan et al. [9] propose to fill in the missing coefficients in the wavelet domain by the total variation (TV) minimization method and evolving the associated PDE numerically, which is relatively slow. To speed up, many fast numerical methods designed for the TV denoising problem are applied to solve the transform domain inpainting problem and some efficient algorithms are obtained. A fast optimization transfer algorithm (OTA) is proposed by Chan et al. [7], in which Chambolle's fast dual projection algorithm [6] is used to solve the TV denoising subproblem. Later Chan et al. [8] propose to use the alternating direction method (ADM) to solve the TV wavelet inpainting model. The latter is more efficient. A primal-dual type numerical algorithm is proposed by Wen et al. [33] to solve the TV wavelet inpainting problem and the convergence is proved. Another primal-dual hybrid gradient method is proposed by Ye and Zhou [37]. Zhang and Chan [40] propose to use the nonlocal TV (NLTV) regularization in wavelet inpainting instead of TV, which greatly improves the image quality than the TV based methods for texture images.

The Fourier domain inpainting problem has been widely addressed in the MR imaging problem that is also termed as Compressed Sensing. Goldstein and Osher [17] propose to use the TV regularization in the Fourier domain inpainting problem and develop a fast numerical scheme based on the split Bregman method. Chen et al. [10] propose two fast algorithms based on the primal-dual hybrid gradient method. Ma et al. [26] propose a model with both TV and wavelet regularization, and derive an efficient numerical algorithm using the operator splitting technique. Guo et al. [20] use both total generalized variation (TGV) and shearlet as regularization terms. A fast numerical algorithm is derived based on the alternating direction method of multiplier (ADMM). The NLTV regularization is adopted by Zhang et al. [39], and an efficient algorithm is proposed using the Bregmanized operator splitting technique. Li and Zeng [24] propose a promising decoupled method for both wavelet and Fourier transform domain inpainting based on the BM3D filter [12].

Image inpainting can also be regarded as a matrix completion problem since the image or its coefficients under certain transform are usually stored as a digital matrix. Low rank matrix completion has attracted considerable interest recently [3,5,22,30,31,34]. As nuclear norm is the convex surrogate of the rank function of matrices, it is widely used as a regularization term in the low rank matrix completion problem. Cai et al. [3] propose the singular value thresholding (SVT) algorithm for the nuclear norm minimization problem. Accelerating numerical methods are proposed in [30,31,34]. However, since most images are not low rank, these low rank based matrix completion methods usually can not produce satisfactory results for the image inpainting problem. Hu et al. [22] propose a new truncated nuclear norm regularization which works well for image inpainting. Generally speaking, there are many nonlocal similar patches in a natural image. Hence the matrix obtained by stacking the nonlocal similar patch vectors should be a low rank matrix and has sparse singular values. Based on this observation, Gu et al. [18] propose a weighted nuclear norm minimization (WNNM) method which works on local patches for image denoising. It is reported that the WNNM method outperforms many state-of-the-art denoising algorithms including BM3D.

The contribution of this paper is two-fold. Firstly, we derive the matrix representation for patch-based WNNM (PWNNM) decomposition and reconstruction operators. Then we reformulate the PWNNM denoising process into three basic steps: image decomposition, patch matrix denoising, and image reconstruction. With these integrated formulation, PWNNM can be regarded as a regular regularization method and can be used in many image processing problems. Secondly, we propose a new method using PWNNM regularization for both image domain inpainting and transform domain inpainting. The main idea is to decouple the original problem into two alternating steps: PWNNM denoising and linear combination in image domain or transform domain. Different from the existing coupled variational methods in which only one energy functional is essentially involved, the proposed method minimize two different energy functionals alternatingly. One advantage of this decoupled method is that the original problem is split into two relatively independent step, such that we have more flexibility in the choice of method for each step. The experimental results demonstrate that the proposed method is competitive with the state-of-the-art inpainting algorithms in terms of PSNR index and visual quality.

The remainder of this paper is organized as follows. In Section 2, we derive the variational formulation of PWNNM. In Section 3, we propose our decoupled method for image inpainting and study the convergence of the iterative algorithm. In Section 4, we display some experimental results and comparisons to illustrate the effectiveness of our method. Finally, we conclude the paper in Section 5.

2. The variational formulation of PWNNM

The PWNNM method is proposed in [18] for image denoising. The main idea is to apply WNNM on many matrices formed by similar patches in the image. This method is very effective especially for high level Gaussian noise. In this section, we derive the variational formulation of PWNNM which includes three steps: image decomposition, patch matrix denoising and image reconstruction. This formulation has not been presented in the existing work so far as we know.

Let us introduce some notations. Suppose U, F and ξ are $n \times n$ matrices representing the ideal image, noisy image and Gaussian additive noise respectively, such that

$$F = U + \xi.$$

The image denoising problem is to recover U from the given data F.

2.1. Image decomposition

Assume that u and f are the corresponding vectors in $\mathbb{R}^N (N = n^2)$ by stacking U and F column by column. To each image patch with size $p \times p (p \ll n)$, we assign its index to be the same as the index of the pixel in its upper-left corner. Define P_j as a $p^2 \times N$ matrix with elements 0 and 1 indicating which elements of u belongs to the jth patch, then we have that the vector obtained by stacking the jth patch column by column is $u_j = P_j u$. We extract R key patches by sliding window in the whole image. For each key patch, in a large enough local window, we can search for K most similar patches by comparing the Euclidean distance of the corresponding vectors. Then all indexes of the image patches are clustered into R groups denoted by $G = \{G_1, G_2, \ldots, G_R\}$, where each group contains the indexes of the K most similar patches $J_r = \{j_{r,1}, \ldots, j_{r,K}\}, r = 1, \ldots, R$. Define the matrix Φ_r as

$$\Phi_r = \begin{bmatrix} P_{j_r,1} \\ \vdots \\ P_{j_r,K} \end{bmatrix} \in \mathbb{R}^{Kp^2 \times N}.$$

Then $\Phi_r u$ extracts the rth group patches of image U by stacking them into a column. The image decomposition matrix Φ is then defined as

$$\Phi = \begin{bmatrix} \Phi_1 \\ \vdots \\ \Phi_R \end{bmatrix} \in \mathbb{R}^{RKp^2 \times N}.$$

2.2. Patch matrix denosing

Let us recall the WNNM problem [18]. Assume X and Y are matrices with the same size. The weighted nuclear norm of X is defined as

$$\|X\|_{w,*} = \sum_{i=1}^{s} |w_i \sigma_i(X)|$$

where $\sigma_i(X)$ means the ith singular value of X, $w = (w_1, \ldots, w_s) \geq 0$ denotes the weights assigned to $\sigma_i(X)$ and s is the number of singular values of X. The WNNM problem is

$$\min_X \|X\|_{w,*} + \frac{1}{2}\|X - Y\|_F^2, \tag{1}$$

which aims to find a low rank approximation of the given matrix Y. The WNNM problem is nonconvex in general. In particular, when the weights are in non-descending order, it can be proved that the optimal solution is given by

$$X = \mathcal{A}_w(Y) := U\mathcal{S}_w(\Sigma)V^T, \tag{2}$$

where $Y = U\Sigma V^T$ is the singular value decomposition (SVD) of Y and $\mathcal{S}_w(\Sigma)$ is the weighted soft thresholding function on the diagonal matrix Σ with weight vector w, i.e.,

$$\mathcal{S}_w(\Sigma)_{ii} := \max(\Sigma_{ii} - w_i, 0). \tag{3}$$

Assume u is the image vector. Define $\mathcal{R}$ as the reshaping operator such that

$$\mathcal{R}\Phi_r u = \left[P_{j_r,1}u, \ldots, P_{j_r,K}u\right].$$

That is, $\mathcal{R}$ reshapes a $Kp^2 \times 1$ vector as a $p^2 \times K$ matrix and each column of this matrix denotes a patch in the image. $\mathcal{R}\Phi_r u$ is called a patch matrix for convenience. In a whole, we have R patch matrices with size $p^2 \times K$.

The patch matrix denoising step of PWNNM can be represented by solving the following WNNM problems

$$\min_{d_r} \|d_r\|_{w_r,*} + \frac{1}{2\sigma}\|d_r - \mathcal{R}\Phi_r f\|_F^2, r = 1, \ldots, R, \tag{4}$$

where w_r is the weight vector for the rth group, and the unknown $d_r \in \mathbb{R}^{p^2 \times K}$. Then the solution of (4) is given by

$$d_r = \mathcal{A}_{w_r}(\mathcal{R}\Phi_r f). \tag{5}$$

Define operators

$$\tilde{\mathcal{R}} = \begin{bmatrix} \mathcal{R} & & \\ & \ddots & \\ & & \mathcal{R} \end{bmatrix}, \quad \mathcal{A}_w = \begin{bmatrix} \mathcal{A}_{w_1} & & \\ & \ddots & \\ & & \mathcal{A}_{w_R} \end{bmatrix}.$$

Then a more compact form of (4) is

$$\min_d \|d\|_{w,*} + \frac{1}{2}\|d - \tilde{\mathcal{R}}\Phi f\|_F^2, \tag{6}$$

where we define

$$d = \begin{bmatrix} d_1 \\ \vdots \\ d_R \end{bmatrix} \in \mathbb{R}^{Rp^2 \times K},$$

$$\|d\|_{w,*} := \sum_{r=1}^{R} \|d_r\|_{w,*}.$$

With these notations, the compact form solution for problem (6) is given by

$$d = \mathcal{A}_w(\tilde{\mathcal{R}}\Phi f). \tag{7}$$

2.3. Image reconstruction

After all the patch matrices are denoised by WNNM, we return each patch to its original position in the image by P_j^T, $j \in J_r$. By the definition of Φ_r, we have

$$\Phi_r^T = [P_{j_r,1}^T, \ldots, P_{j_r,K}^T]. \tag{8}$$

Then the image reconstruction matrix $\Psi \in \mathbb{R}^{N \times RKp^2}$ is defined as

$$\Psi = (\Psi_1, \ldots, \Psi_R)$$

where $\Psi_r = W^{-1}\Phi_r^T$ and $W = \sum_r \sum_{j \in J_r} P_j^T P_j$. Here W is a diagonal matrix since each $P_j^T P_j$ is a diagonal matrix with element 0 or 1. The mth diagonal element of $P_j^T P_j$ equals 1 means that the mth pixel belongs to the jth patch; otherwise, it equals 0. The mth diagonal element of matrix $\sum_{j \in J_r} P_j^T P_j$ means the number of patches in the rth group that contains the mth pixel. Hence, the mth diagonal element of matrix W means the total number of patches that contains the mth pixel in all the groups. Therefore, by the image reconstruction operation, the output image value at the mth pixel equals to the mean of all the patches in all groups at that pixel.

Hence the image reconstruction step of PWNNM can be represented by the following minimization problem

$$\min_u \|u - \sum_r \Psi_r \mathcal{R}^T d_r\|_2^2, \tag{9}$$

where $\mathcal{R}^T$ is the conjugate operator of $\mathcal{R}$, i.e., $\mathcal{R}^T$ reshape a $p^2 \times K$ matrix as a Kp^2-dimensional vector by stacking it column by column. The solution of (9) is immediately given by

$$u = \sum_r \Psi_r \mathcal{R}^T d_r = \Psi \tilde{\mathcal{R}}^T d.$$

2.4. The integrated formulation of PWNNM

By the definition of the image decomposition and image reconstruction matrices Φ and Ψ, it can be easily derived that

$$\Phi^T\Phi = \sum_r \Phi_r^T \Phi_r = W, \tag{10}$$

$$\Psi\Psi^T = \sum_r \Psi_r \Psi_r^T = W^{-1} \tag{11}$$

$$\Psi\Phi = \sum_r \Psi_r \Phi_r = \mathcal{I}. \tag{12}$$

Based on the analysis in Sections 2.1–2.3, the whole PWNNM denoising process on image f can be represented as solving the fixed point of the decoupled problems (6) and (9), that is,

$$\sum_r \Psi_r \mathcal{R}^T \mathcal{A}_{w_r} \mathcal{R} \Phi_r f,$$

or in a compact form as

$$\Psi \tilde{\mathcal{R}}^T \mathcal{A}_w \tilde{\mathcal{R}} \Phi f.$$

3. The proposed method

In this section, we propose a decoupled model for image inpaining and derive an iterative algorithm. Convergence of the algorithm is proved under some assumptions.

3.1. The model and algorithm

Generally, the image inpainting problem can be formulated as

$$f = \mathcal{D}\mathcal{T}u + \eta \tag{13}$$

where $\mathcal{T} \in \mathbb{R}^{N\times N}$ is a transform, $\mathcal{D} \in \mathbb{R}^{t\times N}$ is the downsampling matrix containing $t < N$ rows of the identity matrix of order N, $\eta \in R^t$ is the additive noise, $f \in R^t$ is the acquired incomplete data, $u \in \mathbb{R}^N$ is the ideal image to be recovered [37]. We consider three choices of $\mathcal{T}$: identity transform, wavelet transform and Fourier transform. In all cases, we have

$$\mathcal{T}^T\mathcal{T} = \mathcal{I} \tag{14}$$

where $\mathcal{I}$ is the identity matrix. Note that when $\mathcal{T}$ is the identity matrix, it becomes the image domain inpainting problem. When $\mathcal{T}$ is wavelet transform or Fourier transform, it is transform domain inpainting problem.

In this paper, our motivation is to make use of the fixed point of PWNNM to get a prior for the clean image and apply it to solve the image inpainting problem. Inspired by the variational formulation of PWNNM which have essentially decoupled energies (4) and (9), we propose the following decoupled model for image inpainting

$$\begin{aligned} d &= \arg\min_d \|d\|_{w,*} + \frac{1}{2}\|d - \tilde{\mathcal{R}}\Phi u\|_F^2, \\ u &= \arg\min_u \|u - \Psi\tilde{\mathcal{R}}^T d\|_2^2 + \frac{\mu}{2}\|\mathcal{D}\mathcal{T}u - f\|_2^2, \end{aligned} \tag{15}$$

where $w = \{w_r, r = 1, \ldots, R\}$ are the given weight vectors with nonnegative elements in ranged non-descending order, and μ is a positive balance parameter.

The solution of the d-subproblem is given by (7) in Section 2.2. Denote $\tilde{u} = \Psi\tilde{\mathcal{R}}^T\mathcal{A}_w\tilde{\mathcal{R}}\Phi u$. It is easy to get that $\tilde{u}$ is the fixed point of PWNNM problem for the given image u. Therefore, in the u-subproblem of (15), we have $\|u - \Psi\tilde{\mathcal{R}}^T d\|_2^2 = \|u - \tilde{u}\|_2^2$. In fact, this term can be regarded as a prior for the clean image. It means that the desired clean image is expected to be close to its PWNNM fixed point in the L_2 distance. To show the effectiveness of this prior, we display in Fig. 1 the histograms of the difference $u - \tilde{u}$ for the three test images in Fig. 2, respectively. We can observe that in Fig. 1 for each image the difference values are mostly near zero and follow gaussian distributions approximately. Hence, the L_2 norm distance is a good measure for the difference.

In terms of game theory, problem (15) can be interpreted as a game of two players identified with two variables d and u, respectively [15]. The interaction between the two players are noncooperative since they have different objective functions and generally minimize one will increase the other. The equilibrium of this game is called Nash equilibrium, which is the fixed point (d^*, u^*) of problem (15).

For the u-subproblem, it is easy to derive the closed-form solution

$$u = \left(1 + \mu\mathcal{T}^T\mathcal{D}^T\mathcal{D}\mathcal{T}\right)^{-1}\left(\Psi\tilde{\mathcal{R}}^T d + \mu\mathcal{T}^T\mathcal{D}^T f\right). \tag{16}$$

Since

$$\left(1 + \mu\mathcal{T}^T\mathcal{D}^T\mathcal{D}\mathcal{T}\right)^{-1} = \left(\mathcal{T}^T(1 + \mu\mathcal{D}^T\mathcal{D})\mathcal{T}\right)^{-1} = \mathcal{T}^{-1}\left(1 + \mu\mathcal{D}^T\mathcal{D}\right)^{-1}\mathcal{T},$$

we can rewrite (16) as

$$u = \mathcal{T}^{-1}M^{-1}\mathcal{T}\left(\Psi\tilde{\mathcal{R}}^T d + \mu\mathcal{T}^T\mathcal{D}^T f\right) \tag{17}$$

where $M = 1 + \mu\mathcal{D}^T\mathcal{D}$.

By solving the two subproblems in (15) alternatingly, we can get an iterative algorithm as described in Algorithm 1.

Applying $\Psi\tilde{\mathcal{R}}^T$ on (18) and letting $v^{k+1} = \Psi\tilde{\mathcal{R}}^T d^{k+1}$, we get a variant of the iteration formulas (18) and (19) in Algorithm 1 as follows

Algorithm 1 .

- Initialization: u^0.
- For $k = 0, 1, 2, \ldots$, repeat until stoping criterion is reached

$$d^{k+1} = \mathcal{A}_w(\tilde{\mathcal{R}}\Phi u^k), \tag{18}$$

$$u^{k+1} = \mathcal{T}^{-1}M^{-1}\mathcal{T}\left(\Psi\tilde{\mathcal{R}}^T d^{k+1} + \mu\mathcal{T}^T\mathcal{D}^T f\right). \tag{19}$$

- Output: u^{k+1}.

$$v^{k+1} = \Psi\tilde{\mathcal{R}}^T\mathcal{A}_w(\tilde{\mathcal{R}}\Phi u^k), \tag{20}$$

$$u^{k+1} = \mathcal{T}^{-1}M^{-1}\mathcal{T}\left(v^{k+1} + \mu\mathcal{T}^T\mathcal{D}^T f\right). \tag{21}$$

Since $\mathcal{D}$ is the downsampling matrix with elements 0 and 1, $1 + \mu\mathcal{D}^T\mathcal{D}$ is a diagonal matrix with diagonal elements 1 and $1 + \mu$, thus $\left(1 + \mu\mathcal{D}^T\mathcal{D}\right)^{-1}$ is also a diagonal matrix with diagonal elements 1 and $\frac{1}{1+\mu}$. In (21), $\mathcal{T}^T\mathcal{D}^T f$ denotes the reconstructed image from the incomplete data f directly which is called back projection. Hence, the updating formula of u in (21) can be seem as a linear combination of v and $\mathcal{T}^T\mathcal{D}^T f$. That is,

$$u = \begin{cases} v, & \text{missing coefficents,} \\ \dfrac{v + \mu\mathcal{T}^T D^T f}{1+\mu}, & \text{selected coefficients.} \end{cases} \tag{22}$$

Henceforth, the two steps (20) and (21) can be interpreted as PWNNM denoising and linear combination, respectively.

The advantage of the proposed decoupled method is that the two steps are fully separated such that we have the flexibility to choose the method in each step. For example, we can use the other denoising method in the first step or consider hard constraint in the second step, that is,

$$u = \begin{cases} v, & \text{missing coefficents,} \\ \mathcal{T}^T D^T f, & \text{selected coefficients.} \end{cases} \tag{23}$$

Moreover, we can consider the inpainting problem for incomplete images with blur by introducing a deblurring step in a similar way. Another advantage of this decoupled algorithm is that it provides a framework of how to use PWNNM as a general regularization method in variational methods.

3.2. Convergence analysis

Substituting (18) into (19), we get that the iteration formula of u is

$$u^{k+1} = \mathcal{T}^{-1}M^{-1}\mathcal{T}\left(\Psi\tilde{\mathcal{R}}^T\mathcal{A}_w\tilde{\mathcal{R}}\Phi u^k + \mu\mathcal{T}^T\mathcal{D}^T f\right). \tag{24}$$

Let $\omega^k = \Phi u^k$ and introduce the following linear operator

$$\omega^{k+1} := \mathcal{H}(\omega^k) = \Phi\mathcal{T}^{-1}M^{-1}\mathcal{T}\left(\Psi\tilde{\mathcal{R}}^T\mathcal{A}_w\tilde{\mathcal{R}}\omega^k + \mu\mathcal{T}^T\mathcal{D}^T f\right).$$

Define operators

$$\mathcal{H}_1 = \Phi\mathcal{T}^{-1}M^{-1}\mathcal{T}\Psi \text{ and } \mathcal{H}_2 = \tilde{\mathcal{R}}^T\mathcal{A}_w\tilde{\mathcal{R}}.$$

It is easy to get that

$$\|H(\omega) - H(\tilde{\omega})\|_2 = \|\mathcal{H}_1\mathcal{H}_2(\omega - \tilde{\omega})\|_2.$$

Then $\mathcal{H}$ is a non-expansive operator if both $\mathcal{H}_1$ and $\mathcal{H}_2$ are non-expansive. In the following we study the non-expansiveness of operators $\mathcal{H}_1$ and $\mathcal{H}_2$, respectively.

Proposition 1. *Assume that the weights $w = \{w_r, r = 1, \ldots, R\}$ are vectors with equal elements. For any $\omega, \tilde{\omega}$ in the range of $\mathcal{H}_2$, we have*

$$\|\mathcal{H}_2(\omega) - \mathcal{H}_2(\tilde{\omega})\|_2 \le \|\omega - \tilde{\omega}\|_2. \tag{25}$$

The equality holds if and only if $\mathcal{H}_2(\omega) - \mathcal{H}_2(\tilde{\omega}) = \omega - \tilde{\omega}$.

Proof. According to [25, Lemma 1], the operators $\mathcal{A}_{w_r}, r = 1, \ldots, R$ are non-expansive. Then $\mathcal{A}_w$ is non-expansive. By the definition of $\tilde{\mathcal{R}}$ and $\mathcal{H}_2$, we have

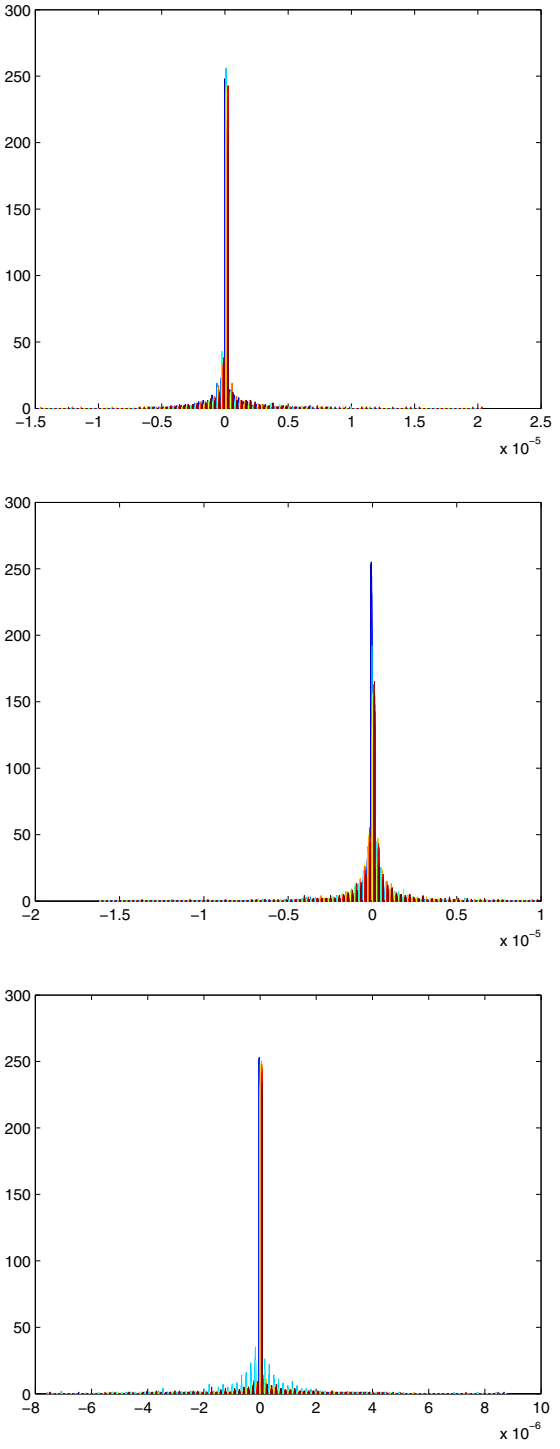

Fig. 1. The histograms of the difference $u - \Psi\tilde{\mathcal{R}}^T d$ in (15) for the three test images House, Barbara and Slope, respectively.

$$
\begin{aligned}
&\|\mathcal{H}_2(\omega) - \mathcal{H}_2(\tilde{\omega})\|_2 \\
&= \|\tilde{\mathcal{R}}^T \mathcal{A}_w \tilde{\mathcal{R}}(\omega - \tilde{\omega})\|_2 \\
&= \|\mathcal{A}_w \tilde{\mathcal{R}}(\omega - \tilde{\omega})\|_F \\
&\le \|\tilde{\mathcal{R}}(\omega - \tilde{\omega})\|_F \\
&= \|\omega - \tilde{\omega}\|_2
\end{aligned}
$$

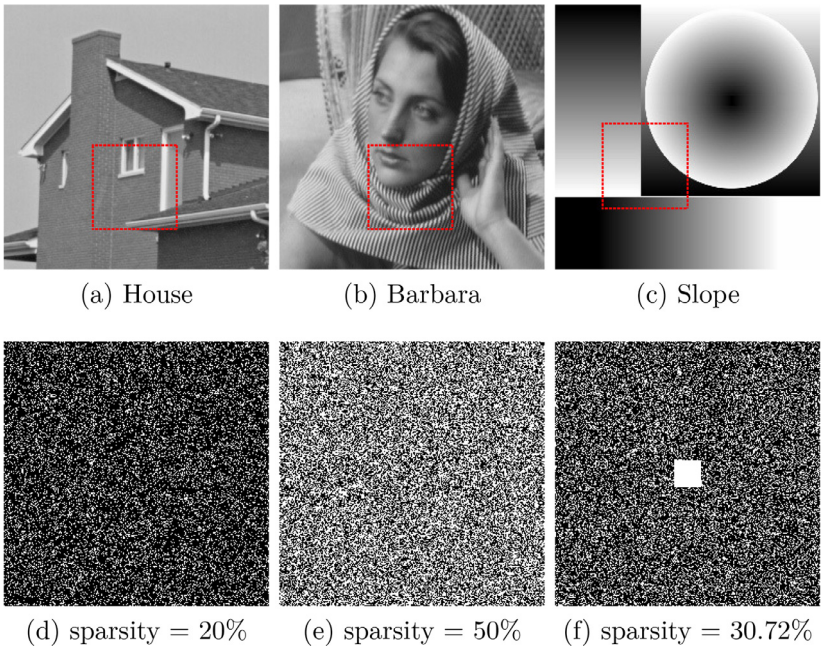

Fig. 2. Test images and inpainting masks with missing data marked in black. (a) House; (b) Barbara; (c) Slope; (d) Image domain mask; (e) Wavelet domain mask; (f) Fourier domain mask.

where the inequality is resulted by the non-expansiveness of $\mathcal{A}_w$. The equality holds if and only if

$$\mathcal{A}_w\tilde{\mathcal{R}}(\omega-\tilde{\omega})=\tilde{\mathcal{R}}(\omega-\tilde{\omega}).$$

Therefore, we get that the equality holds if and only if

$$\mathcal{H}_2(\omega)-\mathcal{H}_2(\tilde{\omega})=\tilde{\mathcal{R}}^T\mathcal{A}_w\tilde{\mathcal{R}}(\omega-\tilde{\omega})=\tilde{\mathcal{R}}^T\tilde{\mathcal{R}}(\omega-\tilde{\omega})=\omega-\tilde{\omega}.$$

This completes the proof. □

Proposition 2. *Assume that the matrix $Q=\Phi\mathcal{T}^{-1}M^{-1}\mathcal{T}\Psi$ is normal. For any $\alpha,\tilde{\alpha}$ in the range of $\mathcal{H}_1$, we have*

$$\|\mathcal{H}_1(\alpha)-\mathcal{H}_1(\tilde{\alpha})\|_2\le\|\alpha-\tilde{\alpha}\|_2. \tag{26}$$

The equality holds if and only if $\mathcal{H}_1(\alpha)-\mathcal{H}_1(\tilde{\alpha})=\alpha-\tilde{\alpha}$.

Proof. According to [21, Theorem 1.3.22], the matrix AB has the same nonzero eigenvalues as BA. Hence the matrix Q has the same nonzero eigenvalues as $\mathcal{T}^{-1}M^{-1}\mathcal{T}\Psi\Phi=\mathcal{T}^{-1}M^{-1}\mathcal{T}$. Moreover, $\mathcal{T}^{-1}M^{-1}\mathcal{T}$ has the same nonzero eigenvalues as $\mathcal{T}\mathcal{T}^{-1}M^{-1}=M^{-1}$. Hence, we conclude that the spectral radius of Q satisfies $\rho(Q)\le 1$. Since Q is normal, we have $\|Q\|_2=\rho(Q)\le 1$. Then we can deduce that

$$\begin{aligned}&\|\mathcal{H}_1(\alpha)-\mathcal{H}_1(\tilde{\alpha})\|_2\\ =\;&\|Q(\alpha-\tilde{\alpha})\|_2\\ \le\;&\|Q\|_2\|\alpha-\tilde{\alpha}\|_2\\ \le\;&\|\alpha-\tilde{\alpha}\|_2.\end{aligned}$$

Assume that $Q=U^T\Gamma U$ is the eigen-decomposition of Q, where U is an orthogonal matrix and Γ is a diagonal matrix with elements in [0, 1]. If the equality holds, i.e., $\|U^T\Gamma U(\alpha-\tilde{\alpha})\|_2=\|\alpha-\tilde{\alpha}\|_2$, then $\|\Gamma U(\alpha-\tilde{\alpha})\|_2=\|U(\alpha-\tilde{\alpha})\|_2$. Thus we have $\Gamma U(\alpha-\tilde{\alpha})=U(\alpha-\tilde{\alpha})$ due to the property of Γ. Multiplying U^T on both sides of the above equation, we obtain that $\mathcal{H}_1(\alpha)-\mathcal{H}_1(\tilde{\alpha})=\alpha-\tilde{\alpha}$. This completes the proof. □ □

It is obvious that the operator $\mathcal{H}$ is non-expansive since $\mathcal{H}_1$ and $\mathcal{H}_2$ are non-expansive. Based on the similar argument as in [32, Theorem 3.4], we can prove the convergence of the sequence w^k, i.e., there exists a w^* such that

$$\lim_{k\to\infty}w^k=w^*.$$

From the iteration formula of u^k in (24), we have

$$u^{k+1}=\mathcal{T}^{-1}M^{-1}\mathcal{T}\left(\Psi\tilde{\mathcal{R}}^T\mathcal{A}_w\tilde{\mathcal{R}}\omega^k+\mu\mathcal{T}^T\mathcal{D}^Tf\right). \tag{27}$$

Hence the convergence of u^k and d^k follows immediately, i.e.,

$$\begin{aligned}\lim_{k\to\infty} u^{k+1} &= \lim_{k\to\infty} \mathcal{T}^{-1}M^{-1}\mathcal{T}\left(\Psi\tilde{\mathcal{R}}^T\mathcal{A}_w\tilde{\mathcal{R}}\omega^k + \mu\mathcal{T}^T\mathcal{D}^T f\right)\\ &= \mathcal{T}^{-1}M^{-1}\mathcal{T}\left(\Psi\tilde{\mathcal{R}}^T\mathcal{A}_w\tilde{\mathcal{R}}\omega^* + \mu\mathcal{T}^T\mathcal{D}^T f\right)\\ &= u^*,\end{aligned}$$

$$\lim_{k\to\infty} d^{k+1} = \lim_{k\to\infty} \mathcal{A}_w(\tilde{\mathcal{R}}\Phi u^k) = \mathcal{A}_w(\tilde{\mathcal{R}}\Phi u^*) = d^*.$$

Therefore, (d^*, u^*) satisfies

$$d^* = \mathcal{A}_w(\tilde{\mathcal{R}}\Phi u^*), \tag{28}$$

$$u^* = \mathcal{T}^{-1}M^{-1}\mathcal{T}\left(\Psi\tilde{\mathcal{R}}^T d^* + \mu\mathcal{T}^T\mathcal{D}^T f\right) \tag{29}$$

which means that (d^*, u^*) is a fixed point of the decoupled problem (15). Assume that the weight vectors $w = \{w_r, r = 1, \ldots, R\}$ have equal positive elements. In this case the weighted nuclear norm is convex [18]. Then it is straightforward to prove that the decoupled functionals in the proposed model (15) are jointly convex with respect to (d, u). Hence, we can conclude that a fixed point (d^*, u^*) of (15) is also a Nash equilibrium point [15]. We sum up the convergence result in the following theorem.

Theorem 1. *Assume that the fixed point set of problem (15) is nonempty and the matrix Q is normal. For any fixed parameter $\mu > 0$ and any weight vectors $w = \{w_r, r = 1, \ldots, R\}$ with equal positive elements, the sequence $\{(d^k, u^k)\}$ generated by Algorithm 1 converges to a fixed point (d^*, u^*) of problem (15), which is also a Nash equilibrium point.*

Remark that when $\mathcal{T} = \mathcal{I}$, $Q = \Phi M^{-1}\Psi = \Phi M^{-1}W^{-1}\Phi^T$ is a symmetric matrix since M and W are diagonal matrix. Hence, the matrix Q is normal. Therefore, we get the convergence result of the proposed algorithm for image domain inpainting problem immediately for weight vector with equal elements.

When the weight vector is with ascending elements, we do not have the convergence theorem since the nonexpansiveness of $\mathcal{H}_2$ does not hold any more. We leave the proof of the convergence for weight vector with ascending elements as our future work. Actually, after having carried out lots of experiments, we observe that the proposed algorithm is still convergent numerically, which will be shown in the next section.

4. Experimental results

In this section, we apply the proposed decoupled method on several standard test images in which some image pixels are missing or some coefficients in wavelet/Fourier transform domain are missing. The results are compared with some closely related methods.

4.1. Experiments setting

In Fig. 2, we display three test images in the first row and three corresponding downsampling masks in the second row, respectively. The three test images are widely used standard test images that are House, Barbara and Slope. House has many structures and fine details. Barbara is a typical texture image. Slope is piecewise smooth with sharp edges. The red rectangle regions will be enlarged for detail comparison in the following. In the second row, masks Fig. 2d–f are for image domain, wavelet transform domain and Fouriers transform domain, respectively. 20% randomly chosen pixels are known in the mask Fig. 2d, 50% randomly chosen coefficients are known in the mask Fig. 2e and 30.72% coefficients are known in the mask Fig. 2f. Note that these kinds of random masks are usually adopted in literatures [10,14,39,40]. We use the model (13) to simulate the incomplete data. In the case of wavelet domain inpainting, $\mathcal{T}$ is set as the wavelet transform with the "daubcqf(6)" basis and 2 levels decomposition using Rice wavelet toolbox 2.4. In all tests, Gaussian noise with zero mean and standard deviation 1 is added.

Cubic interpolation based on Delaunay triangulation (implemented by MATLAB routine "griddata") is used to initialize u^0 in image domain inpainting. For Fourier domain inpainting, we set u^0 as the result of back projection (BP) $\mathcal{T}^T\mathcal{D}^T f$. For wavelet domain inpainting, we initialize u^0 as the cubic interpolation result of $\mathcal{T}^T\mathcal{D}^T f$. These initializations are chosen by experience.

The default parameters of the proposed methods are set as follows. We set $\mu = 10$, patch size $= 9 \times 9$. The key patches are taken by moving the 9×9 window on the image with a step of six pixels.

The weight vector is chosen adaptively for the rth patch matrix, that is,

$$w_{r,i}^k = \frac{\sqrt{2K}}{\sqrt{\max\{\sigma_i^2(\mathcal{R}\Phi_r u^k) - K\sigma^2, 0\}} + \epsilon},$$
$$i = 1, \ldots, \min\{K, p^2\}, r = 1, \ldots, R$$

where σ is the noise standard deviation, σ_i is the i-th singular value and $\epsilon = 10^{-16}$ is to avoid dividing by zero. σ is the key parameter for denoising step which needs to be estimated. To enhance the inpainting speed, we decrease σ from 15, 10,

8, 5 to 2 gradually in the iteration since the noisy extent are decreasing in the iteration process. We perform 30 iterations for each $\sigma \in \{15, 10, 8, 5, 2\}$ and the rest iterations for $\sigma = 2$ or $\sigma = 1$ (the better result is chosen). The stopping criterion of the proposed method is set as the relative error (ReErr) between the successive iterate of the restored image should satisfy the following inequality

$$\text{ReErr} = \frac{\|u^{k+1} - u^k\|_2}{\|u^{k+1}\|_2} < \beta$$

where β is a very small number. For the other compared methods, we use the parameter setting following the original papers.

All the experiments are performed under Windows 8 and MATLAB R2012a with Intel Core i7-4500 CPU@1.80GHz and 8GB memory. The programming language is mixed MATLAB and C for NLTV and BM3D based methods, while it is MATLAB for all the other algorithms.

4.2. Image domain inpainting

We test the House image with randomly 80% of its pixels missing in Fig. 3. Our method is compared with cubic interpolation and three state-of-the-art methods: the sparsity based method MCA [14], the smooth ordering patch based method SOP [27] and the IDI-BM3D inpainting method [23].

Fig. 3b shows the degraded image of Fig. 2a with randomly 80% pixels missing. Fig. 3b, c and g–i shows the results of cubic interpolation, MCA, SOP, IDI-BM3D and the proposed method. In the second and fourth rows, a small rectangle region marked in Fig. 2a by red is enlarged for detail comparison. We observe that the structures and texture details are better recovered by IDI-BM3D in Fig. 3h and by the proposed method in Fig. 3i. In terms of PSNR, the proposed method achieves the highest PSNR value which is about 4.33 dB higher than MCA, 1.20 dB higher than SOP and 0.26dB higher than IDI-BM3D. The parameters of the proposed method is $\beta = 10^{-4}$, iteration=205. This test shows that the proposed method does good work in recovering structure and fine details in the image.

4.3. Transform domain inpainting

For wavelet domain inpainting and Fourier domain inpainting, we compare our results with the following methods without regularization or with different kinds of regularization: the BP method, the TV based method ADM [8], the NLTV based method [39], the decoupled tight frame (TF) method, and the decoupled IDI-BM3D method [24]. Note that in TF, by using the similar method as in this paper, we decouple the image inpainting problem as tight frame denoising by thresholding and linear combination, which is a generalization of [4].

In Fig. 4, Barbara is tested for wavelet domain inpainting. The inpainting results by BP, ADM, NLTV, TF, IDTDI-BM3D and the proposed method are displayed in Figs. 4a–c and Figs. 4g–i, respectively. In the second and fourth rows a small region marked by red in Fig. 2b is enlarged for detail comparison. It is obvious that BP has the poorest result, ADM and TF oversmooth the textures. NLTV recovers more textures than BP, ADM and TF. IDTDI-BM3D and the proposed method recover the textures much better than others and have similar visual quality. For quantitative comparison, the PSNR values of each method are reported below the figures. Exclude BP, ADM has the lowest PSNR value. TF has slightly higher PSNR value than ADM. Among all, the proposed method achieves the highest PSNR value, which is about 8.17dB higher than ADM, 7.15dB than TF, 3.75dB higher than NLTV, and 1.92dB higher than IDTDI-BM3D. This test shows that the proposed method is good at recovering textures.

In Fig. 5, we test Slope for Fourier domain inpainting. In Figs. 5a–c and Figs. 5g-i, we display the results of BP, ADM, NLTV, TF, IDTDI-BM3D and the proposed method, respectively. A small region marked by red in Fig. 2c is enlarged for detail comparison. It is obvious that the edges and piecewise smooth regions are better recovered by IDTDI-BM3D and the proposed method than those by others. The unpleasing "staircase" effect can be observed in the results of ADM, NLTV and TF. The results of IDTDI-BM3D and our method have similar high visual quality. Among all, the proposed method achieves the highest PSNR value. The PSNR value of our method is about 17.60dB higher than NLTV, 13.44dB higher than ADM, 11.38dB higher than TF and 0.34dB higher than IDTDI-BM3D. In this test, it is shown that the proposed method is also good at recovering piecewise smooth images.

To show the convergence behavior, in Fig. 6, we display the curves of PSNR vs. iteration for five methods including ADM, NLTV, TF, IDTDI-BM3D and the proposed method. Fig. 6a and b are corresponding to the results in Figs. 4 and 5, respectively. Note that we rescale the length of some data in order to compare the curves more properly, which includes ADM, TF, IDTDI-BM3D in Fig. 6a, TF and IDTDI-BM3D in Fig. 6b. For example, in Fig. 6a, the length of TF data is rescaled from 1280 iterations to 1280/4 by taking 1 from the successive 4 iterations. We observe that TF achieves slight higher PSNR values than ADM in both wavelet domain inpainting and Fourier domain inpainting. NLTV is better than ADM and TF for wavelet domain inpainting (see Fig. 6a). However, ADM and TF are better than NLTV for Fourier domain inpainting (see Fig. 6b). In both Fig. 6a and b, IDTDI-BM3D and our proposed method get much higher PSNR values than the other three. Meanwhile, our method achieves slightly higher PSNR than IDTDI-BM3D.

The computational time is reported for each method in Figs. 4 and 5. The proposed method is somewhat time consuming, which takes about 2.5 s for each iteration. Generally, we can get the satisfactory converged results at about 200

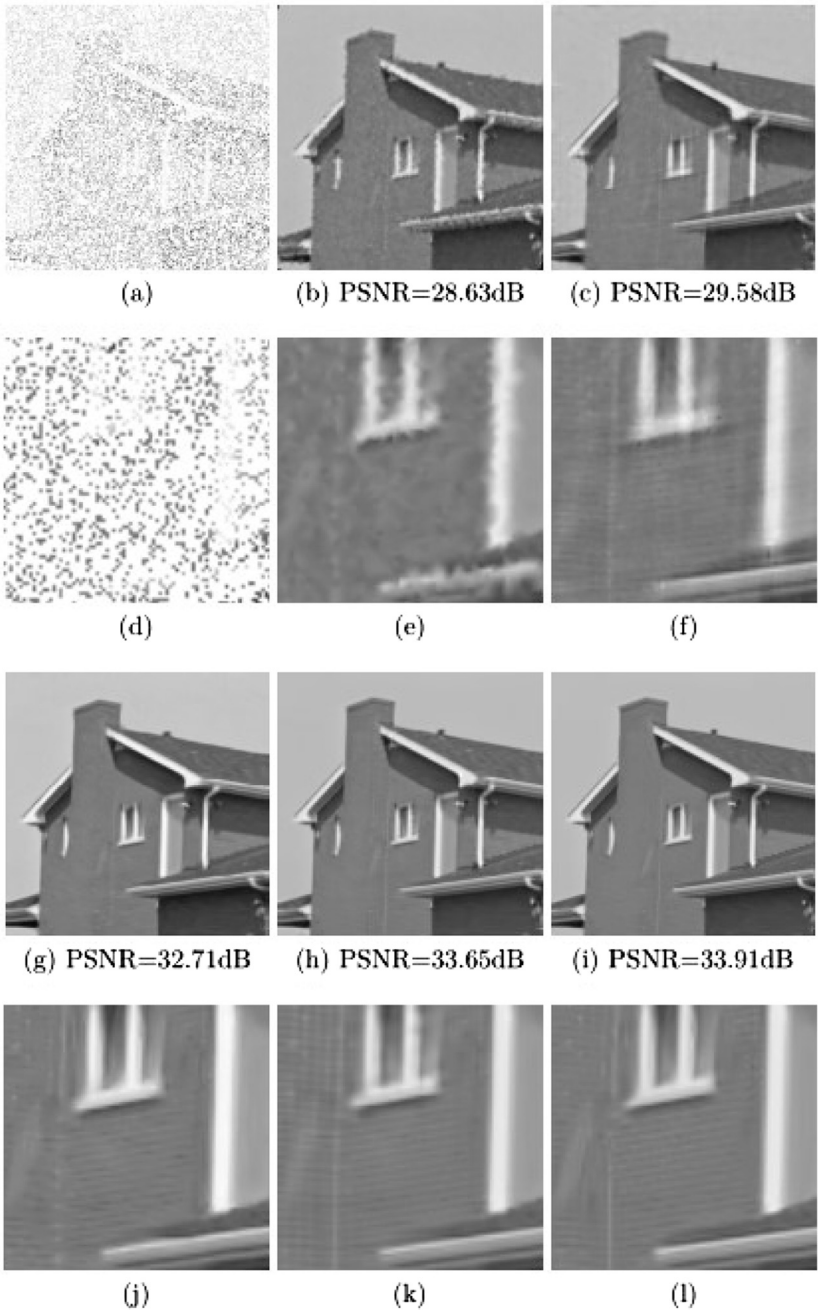

Fig. 3. Image domain inpaiting for House with mask in Fig. 2d, sparsity = 20%: (a) the corrupted image; (b) the result of cubic interpolation; (c) the result of MCA [14]; (d)–(f) the zoomed regions of (a)–(c) respectively; (d) the result of SOP [27]; (e) the result of IDI-BM3D [23]; (f) the result of the proposed method; (j)–(l) the zoomed regions of (g)–(i), respectively.

iterations in all our tests. However, the computational time of the proposed method is compensated by its high quality inpainting results. On the other hand, the computational time of the proposed algorithm can still be reduced by including some parallel computing techniques.

5. Conclusion

In this paper, we have proposed a decoupled method to solve the image inpainting problem in both image domain and transform domain. The inpainting problem has been decoupled as two variational problems: image denoising by PWNNM method and linear combination in image domain or transform domain. The advantage of the decoupled method is that each decoupled problem can be seem as an individual image processing task, which gives us the chance to try different method

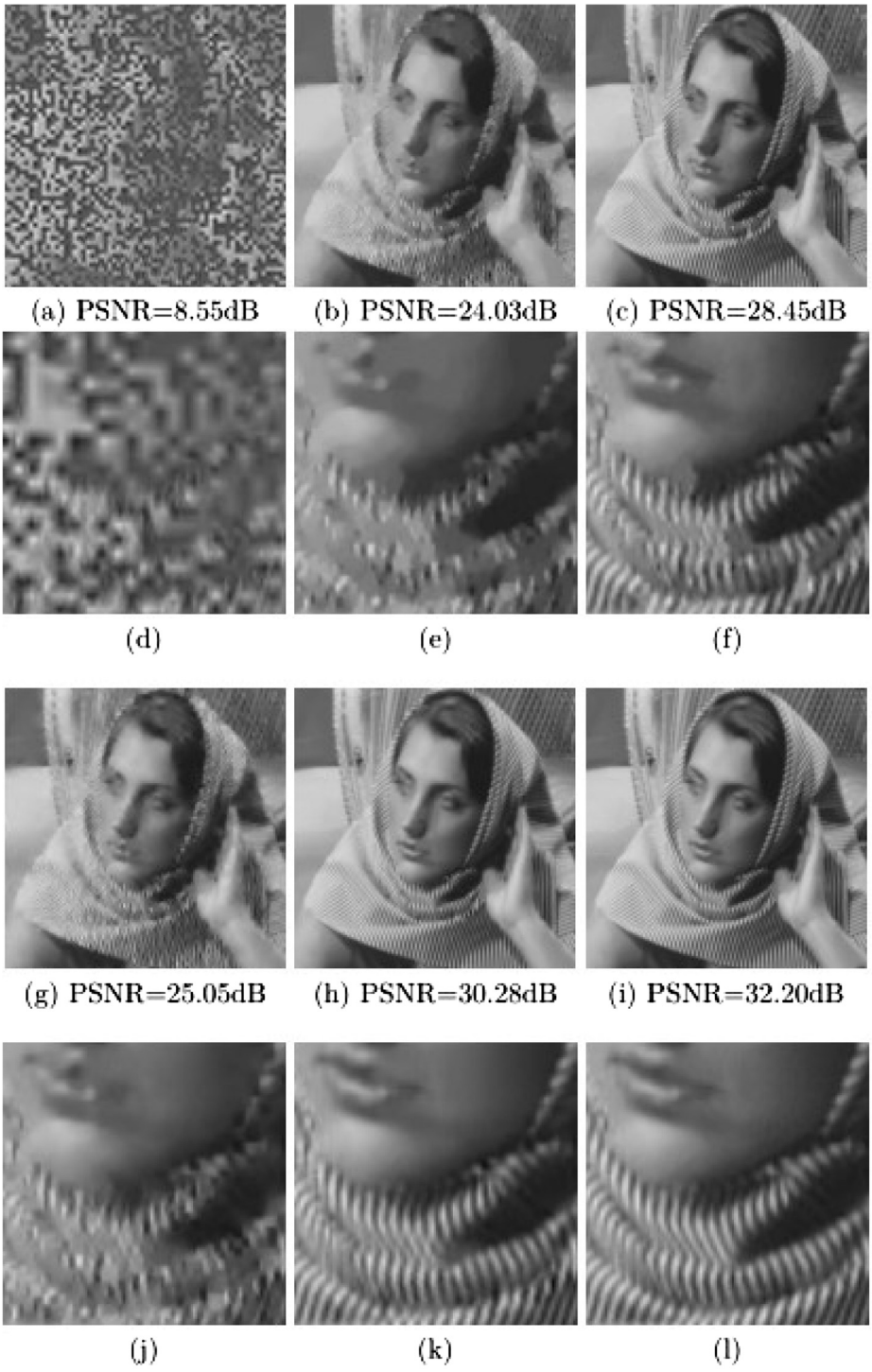

Fig. 4. Wavelet domain inpainting for Barbara with mask in Fig. 2e, sparsity = 50%. (a) the result of BP; (b) the result of ADM [8]: iteration = 594, time = 10.70 s; (c) the result of NLTV: iteration = 250, time =192.88 s; (d)–(f) the zoomed regions of (a)–(c) respectively; (g) the result of TF: iteration = 1280, time = 81.97 s; (h) the result of IDTDI-BM3D [24]: iteration = 500, time = 391.86 s; (i) the result of the proposed method: $\beta = 5 \times 10^{-5}$, iteration = 213, time = 525.48 s; (j)–(l) the zoomed regions of (g)–(i), respectively.

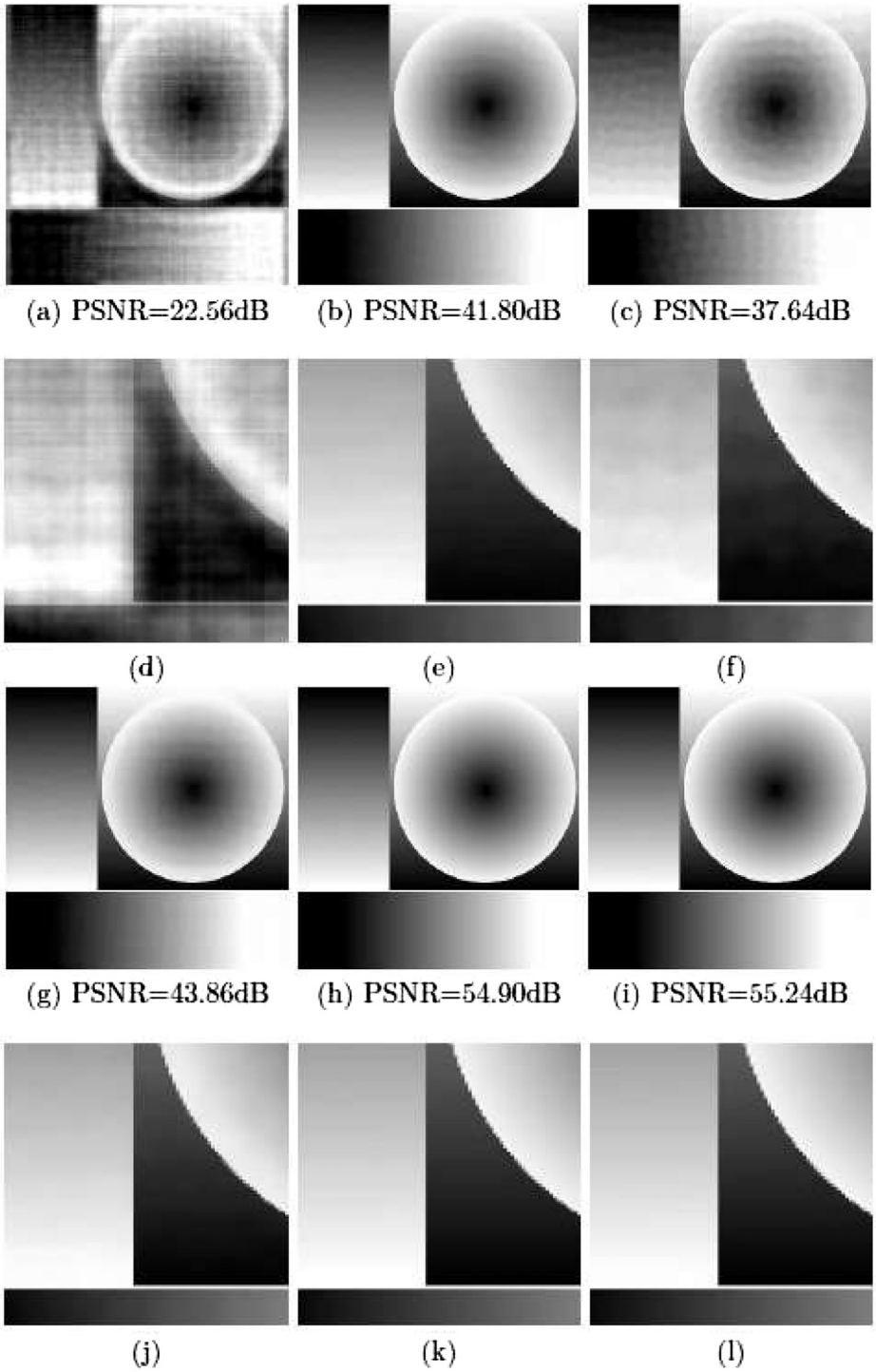

Fig. 5. Fourier domain inpainting for Slope with mask in Fig. 1(f), sparsity = 30.72%. (a) the result of BP; (b) the result of ADM [8]: iteration = 280, time = 6.52 s; (c) the result of NLTV [39]: iteration = 200, time = 452.83 s; (d)–(f) the zoomed regions of (a)–(c), respectively; (g) the result of TF: iteration = 392, time = 24.80 s; (h) the result of IDTDI-BM3D [24]: iteration = 500, time = 426.78 s; (i) the result of the proposed method: $\beta = 10^{-5}$, iteration = 213, time = 498.83 s; (j)–(l) the zoomed regions of (g)–(i), respectively.

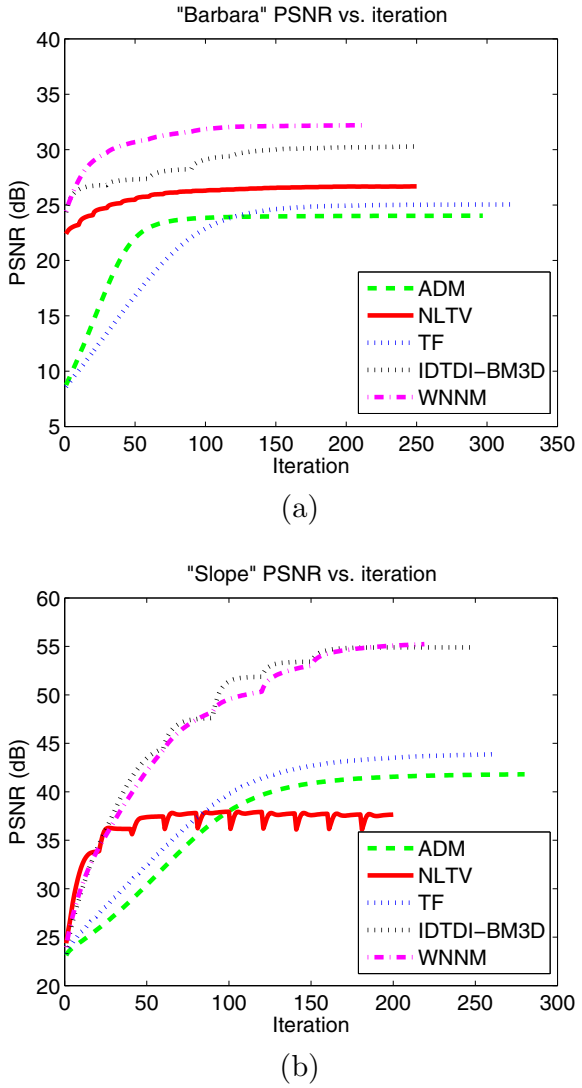

Fig. 6. Convergence behavior. (a) PSNR vs. iteration of the compared methods corresponding to the test in Figs. 4 and 5, respectively.

in each step. In addition, we have derived the variational formulations of PWNNM method such that it can be easily used in other image processing problems as a regularization technique, such as image reconstruction and image segmentation. This will be our future work.

References

[1] M. Bertalmio, G. Sapiro, V. Caselles, C. Ballester, Image inpainting, in: Proceedings of the 27th Annual Conference on Computer Graphics and Interactive Techniques, ACM Press/Addison-Wesley Publishing Co., 2000, pp. 417–424.
[2] A.L. Bertozzi, S. Esedoglu, A. Gillette, Inpainting of binary images using the cahn–hilliard equation, IEEE Trans. Image Process. 16 (1) (2007) 285–291.
[3] J.-F. Cai, E.J. Candès, Z. Shen, A singular value thresholding algorithm for matrix completion, SIAM J. Optim. 20 (4) (2010) 1956–1982.
[4] J.-F. Cai, R.H. Chan, Z. Shen, A framelet-based image inpainting algorithm, Appl. Comput. Harmonic Anal. 24 (2) (2008) 131–149.
[5] E.J. Candès, B. Recht, Exact matrix completion via convex optimization, Found. Comput. Math. 9 (6) (2009) 717–772.
[6] A. Chambolle, An algorithm for total variation minimization and applications, J. Math. Imaging Vis. 20 (1–2) (2004) 89–97.
[7] R.H. Chan, Y.-W. Wen, A.M. Yip, A fast optimization transfer algorithm for image inpainting in wavelet domains, IEEE Trans. Image Process. 18 (7) (2009) 1467–1476.
[8] R.H. Chan, J. Yang, X. Yuan, Alternating direction method for image inpainting in wavelet domains, SIAM J. Imaging Sci. 4 (3) (2011) 807–826.
[9] T.F. Chan, J. Shen, H.-M. Zhou, Total variation wavelet inpainting, J. Math. Imaging Vis. 25 (2006) 107–125.
[10] Y. Chen, W. Hager, F. Huang, D. Phan, X. Ye, W. Yin, Fast algorithms for image reconstruction with application to partially parallel mr imaging, SIAM J. Imaging Sci. 5 (1) (2012) 90–118.
[11] A. Criminisi, P. Pérez, K. Toyama, Region filling and object removal by exemplar-based image inpainting, IEEE Trans. Image Process. 13 (9) (2004) 1200–1212.
[12] K. Dabov, A. Foi, V. Katkovnik, K. Egiazarian, Image denoising by sparse 3-d transform-domain collaborative filtering, IEEE Trans. Image Process. 16 (8) (2007) 2080–2095.

[13] M. Donatelli, D. Martin, L. Reichel, Arnoldi methods for image deblurring with anti-reflective boundary conditions, Appl. Math. Comput. 253 (2015) 135–150.
[14] M. Elad, J.-L. Starck, P. Querre, D.L. Donoho, Simultaneous cartoon and texture image inpainting using morphological component analysis (mca), Appl. Comput. Harmonic Anal. 19 (3) (2005) 340–358.
[15] F. Facchinei, C. Kanzow, Generalized nash equilibrium problems, 4OR 5 (3) (2007) 173–210.
[16] M.-J. Fadili, J.-L. Starck, F. Murtagh, Inpainting and zooming using sparse representations, Comput J 52 (1) (2009) 64–79.
[17] T. Goldstein, S. Osher, The split bregman method for l1-regularized problems, SIAM J. Imaging Sci. 2 (2) (2009) 323–343.
[18] S. Gu, L. Zhang, W. Zuo, X. Feng, Weighted nuclear norm minimization with application to image denoising, in: Proceedings of the 2014 IEEE Conference on Computer Vision and Pattern Recognition (CVPR), IEEE, 2014, pp. 2862–2869.
[19] O.G. Guleryuz, Nonlinear approximation based image recovery using adaptive sparse reconstructions and iterated denoising-part ii: adaptive algorithms, IEEE Trans. Image Process. 15 (3) (2006) 555–571.
[20] W. Guo, J. Qin, W. Yin, A new detail-preserving regularization scheme, SIAM J. Imaging Sci. 7 (2) (2014) 1309–1334.
[21] R.A. Horn, C.R. Johnson, MatrixAnalysis, Cambridge University Press, Cambridge, England, 2012.
[22] Y. Hu, D. Zhang, J. Ye, X. Li, X. He, Fast and accurate matrix completion via truncated nuclear norm regularization, IEEE Trans. Patt. Anal. Mach. Intell. 35 (9) (2013) 2117–2130.
[23] F. Li, T. Zeng, A universal variational framework for sparsity based image inpainting, IEEE Trans Image Process. 23 (10) (2014) 4242–4254.
[24] F. Li, T. Zeng, A new algorithm framework for image inpainting in transform domain, SIAM J. Imaging Sci. 9 (1) (2016) 24–51.
[25] S. Ma, D. Goldfarb, L. Chen, Fixed point and bregman iterative methods for matrix rank minimization, Math. Program. 128 (1–2) (2011) 321–353.
[26] S. Ma, W. Yin, Y. Zhang, A. Chakraborty, An efficient algorithm for compressed mr imaging using total variation and wavelets, in: Proceedings of the IEEE Conference on Computer Vision and Pattern Recognitio, IEEE, 2008, pp. 1–8.
[27] I. Ram, M. Elad, I. Cohen, Image processing using smooth ordering of its patches, IEEE Trans. Image Process. 22 (7) (2013) 2764–2774.
[28] J. Shen, T.F. Chan, Mathematical models for local nontexture inpaintings, SIAM J. Appl. Math. 62 (3) (2002) 1019–1043.
[29] X.-C. Tai, S. Osher, R. Holm, Image inpainting using a tv-stokes equation, in: Image Processing Based on Partial Differential Equations, Springer, Berlin, Heidelberg, 2007, pp. 3–22.
[30] M. Tao, X. Yuan, Recovering low-rank and sparse components of matrices from incomplete and noisy observations, SIAM J. Optim. 21 (1) (2011) 57–81.
[31] K.-C. Toh, S. Yun, An accelerated proximal gradient algorithm for nuclear norm regularized linear least squares problems, Pac. J. Optim. 6 (615–640) (2010) 15.
[32] Y. Wang, J. Yang, W. Yin, Y. Zhang, A new alternating minimization algorithm for total variation image reconstruction, SIAM J. Imaging Sci. 1 (3) (2008) 248–272.
[33] Y.-W. Wen, R.H. Chan, A.M. Yip, A primal–dual method for total-variation-based wavelet domain inpainting, IEEE Trans. Image Process. 21 (1) (2012) 106–114.
[34] Z. Wen, W. Yin, Y. Zhang, Solving a low-rank factorization model for matrix completion by a nonlinear successive over-relaxation algorithm, Math. Program. Comput. 4 (4) (2012) 333–361.
[35] A. Wong, J. Orchard, A nonlocal-means approach to exemplar-based inpainting, in: Proceedings of the 15th IEEE International Conference on Image Processing., IEEE, 2008, pp. 2600–2603.
[36] Z. Xu, J. Sun, Image inpainting by patch propagation using patch sparsity, IEEE Trans. Image Process. 19 (5) (2010) 1153–1165.
[37] X. Ye, H. Zhou, Fast total variation wavelet inpainting via approximated primal-dual hybrid gradient algorithm, Inverse Probl. Imaging 7 (3) (2013) 1031–1050.
[38] G. Yu, G. Sapiro, S. Mallat, Solving inverse problems with piecewise linear estimators: from gaussian mixture models to structured sparsity, IEEE Trans. Image Process. 21 (5) (2012) 2481–2499.
[39] X. Zhang, M. Burger, X. Bresson, S. Osher, Bregmanized nonlocal regularization for deconvolution and sparse reconstruction, SIAM J. Imaging Sci. 3 (3) (2010) 253–276.
[40] X. Zhang, T.F. Chan, Wavelet inpainting by nonlocal total variation, Inverse Probl. Imaging 4 (1) (2010) 191–210.